Nanoscopic mechanism of Cu precipitation at small-angle tilt boundaries in Si

Yutaka Ohno,* Kaihei Inoue, Kentaro Kutsukake, Momoko Deura, Takayuki Ohsawa, and Ichiro Yonenaga
Institute for Materials Research (IMR), Tohoku University, Katahira 2-1-1, Aoba-ku, Sendai 980-8577, Japan

Hideto Yoshida and Seiji Takeda
Institute of Scientific and Industrial Research (ISIR), Osaka University, 8-1 Mihogaoka, Ibaraki, Osaka 567-0047, Japan

Ryo Taniguchi, Hideki Otubo, and Sigeto R. Nishitani
Department of Information, Kwansei Gakuin University, Gakuen 2-1, Sanda, Hyogo 669-1337, Japan

Naoki Ebisawa, Yasuo Shimizu, Hisashi Takamizawa, Koji Inoue, and Yasuyoshi Nagai
Oarai Center, Institute for Materials Research, Tohoku University, Oarai, Ibaraki 311-1313, Japan
(Received 26 December 2014; revised manuscript received 25 May 2015; published 17 June 2015)

We investigate copper (Cu) precipitation at small-angle tilt boundaries on (220) in Czochralski-grown p-type silicon (Si) ingots using transmission electron microscopy, atom probe tomography, and *ab initio* calculations. In the initial stage of precipitation, Cu atoms agglomerate along the boundaries, forming coherent layers (less than about 2 nm thick) of Cu_3Si with a body-centered-cubic structure in a metastable state ($a = 0.285$ nm). As the layers thicken, they become semicoherent with misfit dislocations on the (220) interphase boundaries, reducing coherency strains. Subsequently, the metastable layers convert into incoherent polyhedrons of orthorhombic η''-Cu_3Si in the equilibrium state, forming interphase boundaries on $\{112\}$ in Si. These results are similar to the Cu precipitation processes found in metallic alloys: the formation of Guinier-Preston zones followed by a conversion into the equilibrium θ phase.

DOI: 10.1103/PhysRevB.91.235315 PACS number(s): 61.72.Ff, 64.70.Nd, 68.35.Dv, 73.20.At

I. INTRODUCTION

Polycrystalline materials contain grain boundaries (GBs). A system with GBs involves excess energy because of their structural imperfection, and the amount of energy can be reduced by the nanoscopic structural changes of the GBs via impurity gettering [1–3]. Even though these local changes only occur close to GBs, they play a decisive role in determining the macroscopic properties of most polycrystalline materials, including metals [4,5] and semiconductors [6–8], and in fabricating stable nanostructures [9,10]. Therefore, a comprehensive knowledge of the gettering mechanism is essential for engineering the distributions and sizes of impurity-related nanostructures at GBs in a controlled manner in order to produce cost-effective functional devices [11].

Impurity gettering at GBs is frequently examined in terms of the GB character, which is described using five crystallographic parameters [12]. Among them, the tilt angle is considered to be the most influential parameter with respect to the physical properties of GBs. GBs that have a tilt angle less than about 10°, composed of parallel edge dislocations whose density is determined by the tilt angle [13], are regarded as small-angle tilt boundaries (SATBs). SATBs are frequently introduced in photovoltaic materials, such as silicon (Si) [14]. Even given a small areal fraction, they significantly modify the photovoltaic properties via the contamination of metallic impurities because of their high gettering ability [15–17]. Even though this ability is primarily dominated by the density of the edge dislocations composing the SATBs, it is also influenced by other GB parameters, such as the boundary plane and the twist angle [17,18]. Therefore, we introduce pure SATBs on a specific plane in Si crystals using the Czochralski (CZ) method and examine the intrinsic impurity gettering at the SATBs with high spatial resolution and a low impurity detection limit using transmission electron microscopy (TEM) and atom probe tomography (APT) in combination with *ab initio* calculations.

Because copper (Cu) is a ubiquitous contaminant in Si technologies, we examined Cu precipitation. Cu atoms can be precipitated at heterogeneous nucleation sites, such as SATBs, in crystal growth and thermal processes [19,20]. The η''-phase Cu_3Si precipitates in the equilibrium state at room temperature (RT) [21] are observed at GBs [22]. These precipitates can reduce the minority-carrier diffusion length in solar cells by forming bands of states in the band gap [23], depending on their spatial and size distributions [11]. Furthermore, these Cu-Si systems with nanoscale interfaces have potential applications in spintronics and electronics, such as field emitters and interconnects, passivation, and antireflective layers [24,25], as well as in catalytic oxidation [26]. In this work, we microscopically determine the Cu precipitation conditions at the SATBs, depending on the Cu contamination levels, and propose a nanoscopic mechanism of the precipitation. These findings can aid the control of Cu contaminants using gettering [18,22,27,28], passivation [17], and thermal [29] processes.

II. EXPERIMENTAL

Si ingots (approximately 1 inch in diameter), which were codoped with boron (approximately 0.01 at. %) and Cu (of order 10^{-5} at. %) atoms, were grown with bicrystal seeds using the CZ method. A seed was prepared by combining two square prisms of Si with nearly $\{100\}$ surfaces, and it was pulled along [001] with a rate of 3 μm/s from a melt of granulated boron,

*yutakaohno@imr.tohoku.ac.jp

Cu, and Si. SATBs with a rotation axis of [001] that were parallel to the growth direction were accidentally introduced in an ingot. Small pieces of Si with an SATB were cut from the ingot and annealed at 900 °C for 50 h in a vacuum in order to allow the Cu atoms to diffuse toward the SATB (with a diffusion length of 5 mm). These Si pieces were then cooled to RT at a rate of -1 °C/s.

The atomic structure of Cu precipitates at the SATBs was examined using high-angle annular dark-field (HAADF), high-resolution (HR), and dark-field (DF) TEM (with JEOL JEM-ARM200F and 2000EX microscopes). The damage-free TEM specimens with SATBs were prepared using only mechanochemical etching [30]. A three-dimensional (3D) distribution of Cu atoms at the SATBs was examined using APT, and APT specimens with SATBs were prepared by applying focused-ion-beam (FIB) milling under *in situ* scanning electron microscopy. APT data were obtained using a local electrode atom probe (Ametek, LEAP4000X HR). The ratio of the doubly charged state to the singly charged one for Si exceeded 150 [31]. Furthermore, the 3D distribution of Cu atoms was determined by the Integrated Visualization and Analysis Software (IVAS) protocol [32].

III. RESULTS AND DISCUSSION

A. Cu precipitation conditions in as-grown Si

As can be seen in Fig. 1(a), an SATB in an as-grown ingot was observed using DF-TEM. Most of the boundary segments were on (220) and were composed of an array of parallel dislocations, arranged in intervals of 5–10 nm. Each dislocation extended along the pulling direction of [001], and the Burgers vector, **b**, in which was $a/2[110]$ (i.e., was an edge type). Therefore, the tilt angle of the boundary was approximately 2°–4°, which was confirmed using transmission electron diffraction (not shown). The twist angle was less than 0.2°, indicating a low density of screw dislocations on the boundary.

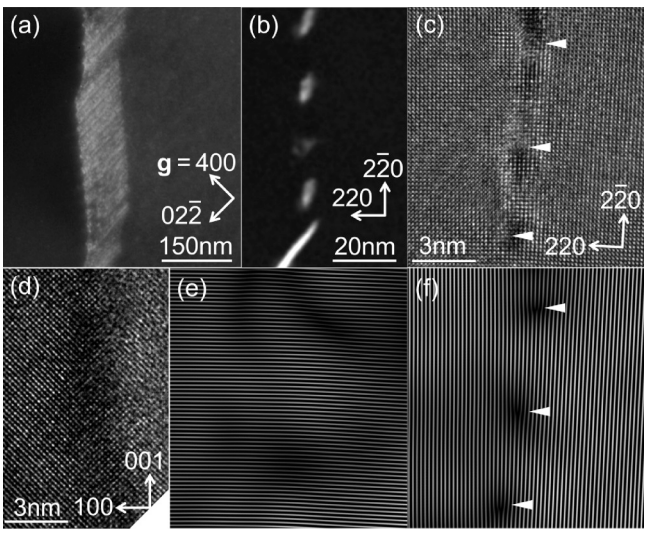

FIG. 1. (a) DF-TEM, (b) HAADF-TEM, and (c), (d) HR-TEM of an SATB in an as-grown crystal. The incident directions are (a) [011], (b), (c) [001], and (d) [010]. The lattice fringes of (e) (2$\bar{2}$0) and (f) (220) were obtained using the Fourier filtering in (c). Arrows in (c) and (f) indicate the edge dislocations that compose the SATB.

Bright dots, which originated from the Cu precipitates, were observed along the SATB shown in Fig. 1(a) using HAADF-TEM [Fig. 1(b)]. Thus, Cu atoms were precipitated at the SATB in the crystal growth process. Moreover, Cu precipitates were observed as a dark band along the SATB, less than about 2 nm in thickness, using HRTEM [Fig. 1(c)]. The image intensity that correlated with the volumes of the Cu precipitates was not uniform along the band because the precipitates distributed inhomogeneously. In particular, intensity was high around the cores of the edge dislocations that composed the SATB. This suggests that Cu atoms were preferentially precipitated around the dislocation cores.

The maximum Cu concentration in the precipitates was estimated to be 75 at. % (72 ± 3 at. % on average) using energy-dispersive x-ray spectroscopy (EDX). The atomic density of the Si in the Cu_3Si precipitates was approximately half the density in Si, which was estimated using electron energy loss spectroscopy. This indicates that the atomic density in the precipitates was approximately twice the height of the density in Si. Furthermore, the precipitates and the Si matrix had similar square lattices in the projections along [001] in the Si matrix. The (2$\bar{2}$0) interphase boundaries were coherent [Fig. 1(e)], even though edge dislocations that composed the SATBs existed [Fig. 1(f)]. A similar square lattice was observed in the [010] projections [Fig. 1(d)]. The square projections of the precipitates differed from those of the orthorhombic Cu_3Si phase in the equilibrium state [21], which is commonly observed at GBs [22]. Considering the similar fourfold symmetries in projections along both [001] and [010], and given an atomic density twice as high as Si, the Cu_3Si precipitates should have a body-centered-cubic (bcc) structure, which is observed in large-angle GBs [33].

B. Cu precipitation conditions in annealed Si

The bcc-Cu_3Si precipitates were developed by annealing [Fig. 2(a)]. In projections along [001] in the Si matrix, even though the precipitates had a square lattice, as in the as-grown crystals, its lattice constant (0.202 nm) was +5% larger when compared with the Si matrix [Fig. 2(b)]. Therefore, misfit dislocations with $\mathbf{b} = a/2[\bar{1}10]$, which were similarly arranged in approximate 5-nm intervals, were introduced along [001] on the (220) interphase boundaries [Fig. 2(c)] and were accompanied with edge dislocations that composed the SATBs [$\mathbf{b} = a/2[110]$ in Fig. 2(d)]. The lattice constant of the stable bcc-Cu_3Si precipitates was estimated to be 0.285 nm ($0.202\sqrt{2}$ nm).

In addition, polyhedral Cu precipitates were observed at the SATBs near a surface in the annealed crystals [Figs. 3(a) and 3(b)]. Although the maximum Cu concentration of 75 at. %, which was estimated using EDX and APT, equaled the maximum in the bcc-Cu_3Si layers, diffraction spots due to the η''-Cu_3Si phase [21] were observed from the polyhedra [Fig. 3(c)]. The volumes of the η'' precipitates increased as the depth from the surface decreased [Fig. 3(b)]. Because of the out-diffusion of the Cu atoms during the cooling process, the Cu contamination level increased as the depth decreased [19]. Therefore, the η'' precipitates should form when the

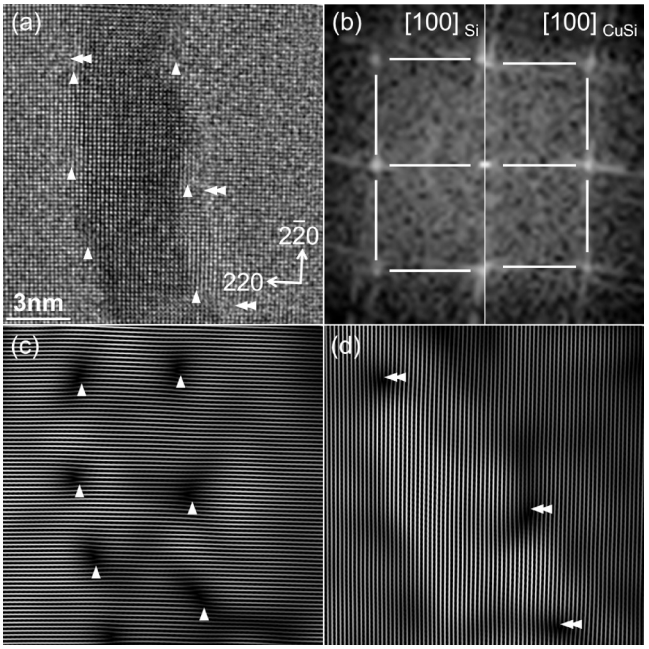

FIG. 2. (a) HRTEM image of an SATB in an annealed crystal for the [001] incident. (b) Fast Fourier transform image for (a). Lattice fringes of (c) $(2\bar{2}0)$ and (d) (220) that were obtained using the Fourier filtering in (a). In (a), (c), and (d), single and double arrows indicate misfit dislocations and the edge dislocations that compose the SATB, respectively.

chemical driving force for precipitation overcomes the barriers for precipitation [34].

The SATBs near the critical depth for the formation of η''-Cu_3Si polyhedrons were examined using APT, and a 3D distribution of the nuclei was clarified. Here, η''-Cu_3Si nuclei, each with an approximate size of 10 nm, were observed on the boundaries [Fig. 4(a)]. They were positioned in similar intervals of approximately 12 nm on a net with mesh basis vectors directed toward [001] and $[\bar{1}11]$ [Fig. 4(b)]. They grew toward the exteriors of the SATBs, forming interphase boundaries that nearly paralleled $\{112\}$ in Si (e.g., the precipitate marked with an asterisk in Fig. 4). Before the η'' phase formed, bcc-Cu_3Si layers with misfit dislocations existed on the SATBs (Fig. 2). Given $\mathbf{b} = a/2\langle 110\rangle$, misfit dislocations should extend on the

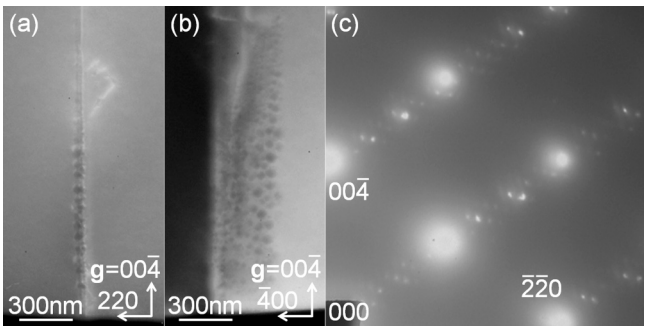

FIG. 3. DF-TEM images of an SATB close to a surface in an annealed crystal for the (a) $[2\bar{2}0]$ and (b) [010] incidents. (c) Diffraction pattern of η''-Cu_3Si polyhedra for the $[2\bar{2}0]$ incident.

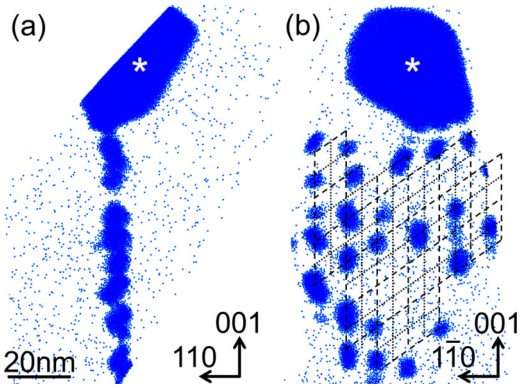

FIG. 4. (Color online) Cu distribution in an APT specimen with an SATB at a depth of approximately 1.5 μm in an annealed crystal viewed (a) parallel to and (b) normal to the boundary. The lattice in (b) corresponds to the misfit dislocation networks on (220) for the bcc-Cu_3Si/Si system. The large precipitate marked with the asterisk is surrounded by $\{112\}$ interphase boundaries.

SATBs along $[1\bar{1}1]$ or $[\bar{1}11]$, as well as along [001]. These dislocations can act as gettering sites for Cu atoms, similarly to the edge dislocations that compose the SATBs [Fig. 1(c)]. The η''-Cu_3Si nuclei should then form on the misfit dislocation networks.

C. Energetic stability of Cu precipitates

The energetic stability of the Cu_3Si phases was investigated using *ab initio* calculations. The η phase, which is in an equilibrium state at high temperatures, is the precursor of the η''-Cu_3Si phase [21]. Therefore, a structural model of bcc-Cu_3Si, based on the Zintl phase [35], and that of the η phase were examined. Given the binary systems of Cu and Si, the model's precipitation energy can be defined as the difference between the model's total energy per atom and the energy of the segregation limit per atom in the chemical composition. Energy was calculated after the outer and inner relaxes of the model occurred using the Vienna *Ab initio* Simulation Package code. The projector augmented wave potential was used, and the cutoff energy was set to 1000 eV [36]. The bcc phase was the most stable with a precipitation energy of -0.01 eV when the lattice constant was 0.29 nm. The calculated constant was close to the lattice constant of 0.285 nm, which was estimated using HRTEM [Fig. 2(b)]. On the other hand, precipitation energy was estimated to be -0.03 eV for the η phase. Therefore, the η phase is more stable than the bcc phase.

The interface energy between a coherent bcc phase and the Si matrix was also calculated. The energy can be defined as $(E_{CuSi/Si} - E_{Si} - E_{CuSi})/S$, in which $E_{CuSi/Si}$ is the total energy of a model with an interphase boundary, and S is the boundary area. Here, E_{Si} represents the total energy of Si whose volume equaled that of Si in the model, and E_{CuSi} represents the total energy of Cu_3Si whose volume equaled that of Cu_3Si in the model. The interface energy of 1.64 J/m^2 for the $\{220\}$ interphase boundaries exceeded the minimum energy of 1.17 J/m^2 for the $\{001\}$ boundaries, but it was

comparable to the energies provided by the high-angle tilt boundaries, excluding Σ 3{111} [37].

D. Mechanism of Cu precipitation at SATBs

In order to discuss the precipitation process of Cu atoms at SATBs, the hypothesis that impurity atoms are precipitated at GBs is imposed, reducing both the strain and GB energies. Therefore, the precipitate's stability can be determined by balancing the precipitation and interface energies for the precipitate and the elastic energy due to lattice mismatch and the edge dislocations that compose the SATBs. The bcc- and η-Cu_3Si phases that have similar atomic densities (approximately 80 nm^{-3}) can induce similar elastic effects in association with their precipitation. With respect to the Si matrix, the bcc phase exhibits good lattice coherency, whereas the η phase is incoherent. Thus, the bcc phase with coherent interphase boundaries, whose interface energy should be lower than that of the η-Cu_3Si/Si incoherent interphase boundaries, can form in the initial stage of Cu precipitation, even though its precipitation energy exceeds that of the η phase. In fact, bcc precipitates were preferentially formed on (100) with the lowest interface energy rather than on (220) [Fig. 1(b)].

The bcc structure can be constructed by introducing Cu atoms into every octahedral and tetrahedral interstitial site in the Si matrix (Cu_{iO} and Cu_{iT}) and substituting the Cu atoms with half of the Si atoms in the lattice sites (Cu_s) without deforming the framework of the Si matrix (Fig. 5). The bcc structure involves the clusters of one Cu_s and three adjacent Cu_{iO}, which was proposed by Shirai *et al.* in [38], with the lowest formation energy in the Cu_4 clusters [39]. Given the lattice mismatch of +5% against the Si matrix, the coherent bcc phase can be formed in a manner that reduces the tensile strains around the SATBs, especially at the cores of the edge dislocations that compose the SATBs [Fig. 1(c)]. This is similar to the oxygen gettering conditions observed at SATBs [41]. When this coherent phase grows and its thickness exceeds a critical value (approximately 2.5 nm, according to the Matthews and Blakeslee equation [40]), coherency strains are relieved by the misfit dislocations with $\mathbf{b} = a/2[\bar{1}10]$, as well as by the edge dislocations, where $\mathbf{b} = a/2[110]$, that compose the SATBs (Fig. 2). Finally, as the Cu atoms agglomerate further, η''-Cu_3Si incoherent precipitates are formed in the thermal equilibrium state (Figs. 3 and 4), presumably by trigonal distortions of the bcc phase [21], forming {112} interphase boundaries, in which the interface energy should exceed that of the bcc-Cu_3Si/Si interphase boundaries. These results are similar to those produced by Cu precipitation processes in metallic alloys, that is, a formation of Guinier-Preston (GP) zones [42,43] followed by a conversion into the θ phase in the equilibrium state.

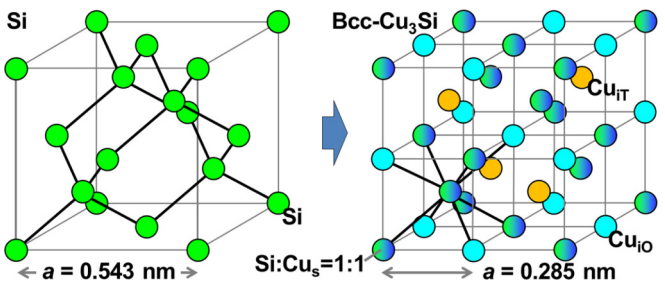

FIG. 5. (Color online) Precipitation model for a semicoherent bcc-Cu_3Si phase. Cu_{iO} or Cu_{iT}, respectively, indicates a Cu atom in an octahedral or tetrahedral interstitial site in the Si matrix. Cu_s signifies that a Cu atom is substituted in a Si lattice site.

It should be noted that the Cu precipitation process at the SATBs somewhat differs from that at the localized nucleation sites, such as the isolated dislocations and point defects. The precipitation ability of these nucleation sites is less than the ability achieved with SATBs [44], and precipitates often accompany the extended defects, such as dislocation loops and stacking faults [45]. This ability is enhanced at the SATBs as a result of the confinement of the tensile strains near the boundary planes because coherent Cu precipitates can preferentially expand along the planar strains. Other metallic impurities, such as iron and nickel, can also preferentially accumulate in the SATBs through similar coherent precipitation mechanisms in the initial stage of their precipitation.

Ab initio calculations revealed that the bcc-Cu_3Si phase acts as a conductor. Therefore, the bcc-Cu_3Si layers may apply to Cu-Si interface nanotechnologies, such as nanoscale field emitters and interconnects. The thicker layers have a high density of misfit dislocations, which are introduced even at low levels of Cu contamination. These thicker layers are candidates for the devastating centers of SATBs with tilt angles of approximately 2°, which are observed in nominally clean crystals used for solar cells [17].

IV. CONCLUSION

Cu precipitation at the SATBs in p-type CZ-Si ingots was investigated at an atomistic level using TEM, APT, and *ab initio* calculations. The precipitation mechanism was explained in terms of a balance between the precipitation and interface energies for the precipitates, as well as in terms of the elastic energy produced by a lattice mismatch and the edge dislocations that compose the SATBs. The precipitation process, which is similar to the formation process of GP zones in metallic alloys, could be a universal phenomenon in noninsulating polycrystalline materials with metallic impurities. This result could help fabricate functional polycrystalline devices via the control of impurity precipitation.

ACKNOWLEDGMENTS

This work was partly supported by JSPS KAKENHI Grant No. 26600038 and the Integrated Materials Research Center for a Low-Carbon Society in IMR (2012-2014). HAADF was performed at ISIR under the Cooperative Research Program of Network Joint Research Center for Materials and Devices. CZ growth of Si:Cu bicrystals, APT measurements, and *ab initio* calculations were performed at IMR, the Oarai Center, and Kwansei Gakuin University, respectively, under the Inter-University Cooperative Research Program in IMR.

[1] M. P. Harmer, Science **332**, 182 (2011).
[2] J. F. Nie, Y. M. Zhu, J. Z. Liu, and X. Y. Fang, Science **340**, 957 (2013).
[3] T. Frolov, S. V. Divinski, M. Asta, and Y. Mishin, Phys. Rev. Lett. **110**, 255502 (2013).
[4] A. King, G. Johnson, D. Engelberg, W. Ludwig, and J. Marrow, Science **321**, 382 (2008).
[5] P. V. Liddicoat, X. Z. Liao, Y. H. Zhao, Y. T. Zhu, M. Y. Murashkin, E. J. Lavernia, R. Z. Valiev, and S. P. Ringer, Nat. Commun. **1**, 63 (2010).
[6] C. Li, Y. Wu, J. Poplawsky, T. J. Pennycook, N. Paudel, W. Yin, S. J. Haigh, M. P. Oxley, A. R. Lupini, M. Al-Jassim, S. J. Pennycook, and Y. Yan, Phys. Rev. Lett. **112**, 156103 (2014).
[7] D. Abou-Ras, B. Schaffer, M. Schaffer, S. S. Schmidt, R. Caballero, and T. Unold, Phys. Rev. Lett. **108**, 075502 (2012).
[8] T. L. Chan, D. West, and S. B. Zhang, Phys. Rev. Lett. **107**, 035503 (2011).
[9] Y. Li, D. Raabe, M. Herbig, P.-P. Choi, S. Goto, A. Kostka, H. Yarita, C. Borchers, and R. Kirchheim, Phys. Rev. Lett. **113**, 106104 (2014).
[10] T. Chookajorn, H. A. Murdoch, and C. A. Schuh, Science **337**, 951 (2012).
[11] T. Buonassisi, A. A. Istratov, M. A. Marcus, B. Lai, Z. Cai, S. M. Heald, and E. R. Weber, Nat. Mater. **4**, 676 (2005).
[12] M. Herbig, D. Raabe, Y. J. Li, P. Choi, S. Zaefferer, and S. Goto, Phys. Rev. Lett. **112**, 126103 (2014).
[13] W. T. Read and W. Shockley, Phys. Rev. **78**, 275 (1950).
[14] K. Kutsukake, M. Deura, Y. Ohno, and I. Yonenaga, Jpn. J. Appl. Phys. (to be published, 2015).
[15] X. Yu, X. Li, R. Fan, D. Yang, M. Kittler, M. Reiche, M. Seibt, and G. Rozgonyi, J. Appl. Phys. **108**, 053719 (2010).
[16] T. Tachibana, J. Masuda, K. Imai, A. Ogura, Y. Ohshita, K. Arafune, and M. Tajima, Jpn. J. Appl. Phys. **48**, 121202 (2009).
[17] J. Chen and T. Sekiguchi, Jpn. J. Appl. Phys. **46**, 6489 (2007).
[18] T. Sameshima, N. Miyazaki, Y. Tsuchiya, H. Hashiguchi, T. Tachibana, T. Kojima, Y. Ohshita, K. Arafune, and A. Ogura, Appl. Phys. Express **5**, 042301 (2012).
[19] A. Autruffe, L. Vines, L. Arnberg, and M. Di Sabatino, J. Crystal Growth **372**, 180 (2013).
[20] T. Buonassisi, A. A. Istratov, M. D. Pickett, M. Heuer, J. P. Kalejs, G. Hahn, M. A. Marcus, B. Lai, Z. Cai, S. M. Heald, T. F. Ciszek, R. F. Clark, D. W. Cunningham, A. M. Gabor, R. Jonczyk, S. Narayanan, E. Sauar, and E. R. Weber, Prog. Photovolt.: Res. Appl. **14**, 513 (2006).
[21] J. K. Solberg, Acta Cryst. A **34**, 684 (1978).
[22] T. Buonassisi, M. A. Marcus, A. A. Istratov, M. Heuer, T. F. Ciszek, B. Lai, Z. Cai, and E. R. Weber, J. Appl. Phys. **97**, 063503 (2005).
[23] X. Yu, J. Lu, and G. Rozgonyi, J. Appl. Phys. **104**, 113702 (2008).
[24] H. Geaney, C. Dickinson, C. O. Dwyer, E. Mullane, A. Singh, and K. M. Ryan, Chem. Mater. **24**, 4319 (2012).
[25] F. W. Yuan, C. Y. Wang, G. A. Li, S. H. Chang, L. W. Chu, L. J. Chen, and H. Y. Tuan, Nanoscale **5**, 9875 (2013).
[26] J. M. E. Harper, A. Charai, L. Stolt, F. M. d'Heurle, and P. M. Fryer, Appl. Phys. Lett. **56**, 2519 (1990).
[27] D. P. Fenning, A. S. Zuschlag, M. I. Bertoni, B. Lai, G. Hahn, and T. Buonassisi, J. Appl. Phys. **113**, 214504 (2013).
[28] M. Seibt, D. Abdelbarey, V. Kveder, C. Rudolf, P. Saring, L. Stolze, and O. Voß, Mater. Sci. Eng. B **159-160**, 264 (2009).
[29] T. Buonassisi, A. A. Istratov, S. Peters, C. Ballif, J. Isenberg, S. Riepe, W. Warta, R. Schindler, G. Willeke, Z. Cai, B. Lai, and E. R. Weber, Appl. Phys. Lett. **87**, 121918 (2005).
[30] Y. Ohno, I. Yonenaga, K. Miyao, K. Maeda, and H. Tsuchida, Appl. Phys. Lett. **101**, 042102 (2012).
[31] Y. Ohno, K. Inoue, Y. Tokumoto, K. Kutsukake, I. Yonenaga, N. Ebisawa, H. Takamizawa, Y. Shimizu, K. Inoue, Y. Nagai, H. Yoshida, and S. Takeda, Appl. Phys. Lett. **103**, 102102 (2013).
[32] B. Gault, D. Haley, F. de Geuser, M. P. Moody, E. A. Marquis, D. J. Larson, and B. P. Geiser, Ultramicrosc. **111**, 448 (2011).
[33] M. Elkajbaji, J. Dessus, and J. Thibault, Philos. Mag. A **66**, 873 (1992).
[34] C. Flink, H. Feick, S. A. McHugo, W. Seifert, H. Hieslmair, T. Heiser, A. A. Istratov, and E. R. Weber, Phys. Rev. Lett. **85**, 4900 (2000).
[35] N. E. Christensen, Phys. Rev. B **32**, 207 (1985).
[36] Y. Yamamoto, K. Togase, Y. Ohno, I. Yonenaga, and S. R. Nishitani, Jpn. J. Appl. Phys. **53**, 061302 (2014).
[37] M. Kohyama, Modell. Simul. Mater. Sci. Eng. **10**, R31 (2002).
[38] K. Shirai, H. Yamaguchi, A. Yanase, and H. Katayama-Yoshida, J. Phys.: Condens. Matter **21**, 064249 (2009).
[39] A. Carvalho, D. J. Backlund, and S. K. Estreicher, Phys. Rev. B **84**, 155322 (2011).
[40] J. W. Matthews and A. E. Blakeslee, J. Crystal Growth **27**, 118 (1974).
[41] Y. Ohno, K. Inoue, K. Fujiwara, M. Deura, K. Kutsukake, I. Yonenaga, Y. Shimizu, K. Inoue, N. Ebisawa, and Y. Nagai, Appl. Phys. Lett. **106** (2015).
[42] A. Guinier, Ann. Phys. (Paris) **12**, 161 (1939).
[43] G. D. Preston, Philos. Mag. **26**, 855 (1938).
[44] O. V. Feklisova, X. Yu, D. Yang, and E. V. Yakimov, Semicond. **47**, 232 (2013).
[45] M. Seibt, M. Griess, A. A. Istratov, H. Hedemann, A. Sattler, and W. Schroter, Phys. Status Solidi A **166**, 171 (1998).